Inertial Stability and Tropical Cyclone Development

WAYNE H. SCHUBERT AND JAMES J. HACK[1]

Department of Atmospheric Science, Colorado State University, Fort Collins 80523

(Manuscript received 14 September 1981, in final form 6 April 1982)

ABSTRACT

We consider the frictionless, axisymmetric, balanced flow occurring in a thermally forced vortex on an f-plane. Following Eliassen (1952) we derive the diagnostic equation for the forced secondary circulation. This equation contains the spatially varying coefficients A (static stability), B (baroclinity), C (inertial stability), and the thermal forcing Q. Assuming that A is a constant, $B = 0$, and that C and Q are piecewise constant functions of radius, we obtain analytical solutions for the forced secondary circulation. The solutions illustrate the following points. 1) For a given Q an increase in inertial stability leads to a decrease in the forced secondary circulation and a change in the radial distribution of local temperature change, with enhanced $\partial\theta/\partial t$ in the region of high inertial stability. 2) Lower tropospheric tangential wind accelerations are larger inside the radius of maximum wind, which leads to a collapse of the radius of maximum wind. 3) The fraction of Q which ends up as $\partial\theta/\partial t$ increases during the tropical cyclone development, particularly if the horizontal extent of Q is small and close to the region of high inertial stability. 4) One can regard the formation of an eye as a process which tends to stabilize the vortex since it removes Q from the protected, highly stable inner region.

1. Introduction

A major conceptual breakthrough in understanding tropical cyclones was provided by Ooyama (1964, 1969a) and Charney and Eliassen (1964) when they demonstrated that cyclone development could occur by a kind of secondary instability involving the cooperative interaction of two scales of motion, the cumulus scale and the cyclone scale. The cumulus clouds were viewed as supplying a radially varying pattern of latent heat release to the cyclone and the cyclone as supplying moisture to the cumulus clouds, primarily through boundary layer convergence. This process, which has become known as CISK, is depicted schematically in Fig. 1. A simple interpretation is as follows. Suppose that at $t = t_0$ we have an anticyclone in the upper troposphere ($\approx$300 mb), a cyclone in the lower troposphere ($\approx$700 mb) above the boundary layer, and an Ekman layer, driven by the same pressure gradient force that exists at 700 mb, in the lowest 100 mb. The moisture convergence in the boundary layer is assumed to support a population of deep, precipitating convective clouds. In the outer regions, where there is boundary layer divergence, there is assumed to be no convection. The boundary layer convergence and the radially varying latent heat release drive the secondary circulation shown in the upper cross-section of Fig. 1. The adiabatic cooling associated with the upward vertical motion does not quite cancel the latent heat release, so there is local warming of the mid-troposphere in the vortex center. Moreover, this warming of the vortex interior is larger than the warming due to subsidence in the outer, non-precipitating region. As shown in the bottom row of Fig. 1, this leads to more intense upper-level anticyclonic and lower level cyclonic circulations, increased boundary-layer convergence, and hence increased latent heat release.

Let us now discuss in more detail the transverse circulation shown in Fig. 1. According to Eliassen's (1952) theory of quasi-balanced vortex flow, the movement of air parcels in the (r, z) plane is forced by heat and angular momentum sources but occurs against two stabilizing factors[2]: static stability, which provides resistance to vertical displacements; and inertial stability, which provides resistance to radial displacements. Static stability can be expressed in terms of N^2, the square of the Brunt-Vaisäla frequency, while inertial stability can be expressed by $[f + (\partial rv/r\partial r)][f + (2v/r)]$, where v is the tangential wind. In linear CISK theory the inertial stability is approximated by f^2, which, for a typical latitude and value of N^2, leads to a Rossby radius of internal deformation of about 1000 km. When the horizontal scale of the convective region is small compared to this Rossby radius, there is little resistance to parcel

[1] Present affiliation: IBM, Thomas J. Watson Research Center, Yorktown Heights, NY 10598.

[2] Here we neglect the effect of baroclinity. In the later stages of tropical cyclone development baroclinity does play an important role, particularly in determining the outward tilt with height of the ascending branch of the transverse circulation.

0022-4928/82/081687-11$06.75

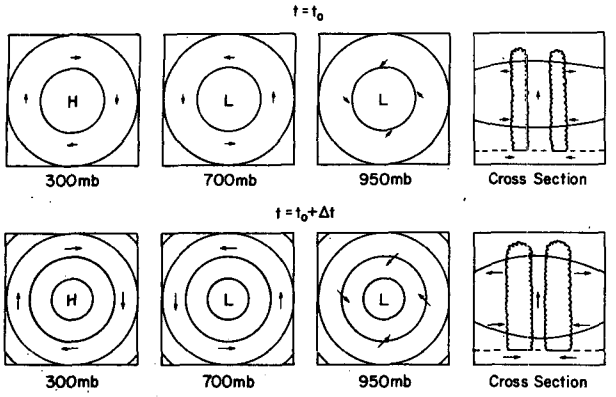

FIG. 1. Schematic depiction of CISK. Initially there is an anticyclone aloft and a cyclone in the lower troposphere. Ekman convergence in the boundary layer provides moisture to a population of precipitating clouds. Most of the diabatic heat source is balanced by the adiabatic cooling associated with the induced transverse circulation. However, there is a slight warming $\partial\theta/\partial t$ and accompanying thickness change, yielding a more intense anticyclone aloft, a more intense cyclone below, increased Ekman convergence, more clouds, etc.

movement in the (r, z) plane and the adiabatic cooling, proportional to N^2w, is nearly as large as the heating due to cumulus convection. Only a small percentage of the convective heating is then left over to warm the column, cause more intense rotational flow, more intense boundary layer convergence and, hence, a more vigorous population of precipitating clouds. If we define "efficiency" as the actual warming of the column, divided by the heating due to convection, we can view linear CISK as an inefficient process. However, observations and numerical experiments with nonlinear primitive equation and balanced models show that only in the very initial phase of tropical cyclone development can the inertial stability be approximated by f^2. During most of the rapid deepening phase $\partial rv/r\partial r$ and $2v/r$ are considerably larger than f in the inner region. This increased inertial stability provides added resistance to the movement of air parcels in the (r, z) plane. For a given latent heating field increased inertial stability thus means reduced N^2w and more efficient warming of the column. Thus, the inertial stability and the efficiency can grow in a nonlinear feedback process. The purpose of this paper is to explore the dynamics of this nonlinear feedback process.

Recently Shapiro and Willoughby (1982) have solved Eliassen's transverse circulation equation for point sources of heat and angular momentum. For an idealized barotropic vortex, an analytical solution was found by the method of images. For more realistic barotropic and baroclinic vortices, numerical solutions were obtained. These analytical and numerical solutions illustrate the tendency for a given source term to produce evolution which is faster for a strong vortex than for a weak vortex. They also show that, in most cases, the tangential wind increases with time most rapidly just inside the radius of maximum wind, which leads to constriction of the radius of maximum wind. In an effort to provide observational evidence for some of these results, Willoughby *et al.* (1981) have analysed recent aircraft observations of hurricanes and typhoons for cycles of intensification and weakening associated with variations in eye diameter. They have found that frequently an outer tangential wind maximum and associated concentric cloud ring will constrict on a pre-existing tangential wind maximum and associated eye, and will eventually replace it. The decay of the inner cloud ring is associated with weakening or at least slower intensification. In one well-documented case (Hurricane Allen, 1980) excellent agreement was found between the tangential wind and geopotential tendencies computed from solutions of Eliassen's transverse circulation equation and the tendencies actually observed.

The analysis presented here is similar in spirit to those of Eliassen (1952), Willoughby (1979), Smith (1981) and Shapiro and Willoughby (1981), i.e., it is a diagnostic analysis and not a closed theory of vortex development (e.g. Ooyama, 1969a,b; Sundqvist, 1970a,b). We derive analytical solutions of Eliassen's transverse circulation equation under the assumptions that the vortex is barotropic, has constant static stability and piecewise constant inertial stability and that the heating is sinusoidal in height and constant in radius within an annular region. Using these solutions in the thermodynamic equation, we then derive relations for the ratio of warming $\partial\theta/\partial t$ to heating Q. Since this ratio can be thought of as a local efficiency of heating, our solutions show how the efficiency depends on the strength of the inertial stability and on the relative horizontal scales of the inertial stability and heating.

2. Governing equations and solutions

Consider the frictionless, axisymmetric, balanced flow occurring in a thermally forced vortex on an f-plane. Using the Hoskins and Bretherton (1972) pseudo-height coordinate $z = [1 - (p/p_0)^\kappa](c_p\theta_0/g)$, the gradient wind balance, conservation of absolute angular momentum, hydrostatic balance, mass continuity (Boussinesq form) and thermodynamic equations can be written

$$m^2 = r^3 \frac{\partial \Phi}{\partial r}, \tag{2.1}$$

$$\frac{dm}{dt} = 0, \tag{2.2}$$

$$\frac{\partial \Phi}{\partial z} = \frac{g}{\theta_0}\theta, \tag{2.3}$$

$$\frac{\partial ru}{r\partial r} + \frac{\partial w}{\partial z} = 0, \tag{2.4}$$

$$\frac{d\theta}{dt} = Q, \tag{2.5}$$

where u, v, w are the radial, tangential and vertical components of velocity, $m = rv + (fr^2/2)$ the absolute angular momentum per unit mass, $\Phi = \phi + (f^2r^2/8)$, $d/dt = \partial/\partial t + u(\partial/\partial r) + w(\partial/\partial z)$, and subscript zero denotes a constant "surface" value. The thermal wind equation is obtained from (2.1) and (2.3). It takes the simple form $(\partial m^2/r^3\partial z) = (g/\theta_0)(\partial\theta/\partial r)$. We now define the streamfunction ψ such that $u = -\partial\psi/\partial z$ and $w = \partial r\psi/r\partial r$. Eliminating local time changes between (2.2) and (2.5) with the aid of the thermal wind equation we obtain the diagnostic equation for the transverse circulation

$$\frac{\partial}{\partial r}\left(A\frac{\partial r\psi}{r\partial r} + B\frac{\partial\psi}{\partial z}\right) + \frac{\partial}{\partial z}\left(B\frac{\partial r\psi}{r\partial r} + C\frac{\partial\psi}{\partial z}\right) = \frac{g}{\theta_0}\frac{\partial Q}{\partial r}, \tag{2.6}$$

where

$$A = \frac{g}{\theta_0}\frac{\partial\theta}{\partial z} \quad \text{(static stability)},$$

$$B = -\frac{g}{\theta_0}\frac{\partial\theta}{\partial r} = -\frac{\partial m^2}{r^3\partial z} \quad \text{(baroclinity)},$$

$$C = \frac{\partial m^2}{r^3\partial r} = \left(f + \frac{\partial rv}{r\partial r}\right)\left(f + \frac{2v}{r}\right) \quad \text{(inertial stability)}.$$

As for boundary conditions we require that ψ vanish on the axis $r = 0$ and on the bottom and top pressure surfaces $z = 0$, z_T and that $\psi \to 0$ as $r \to \infty$.

Eq. (2.6) was first derived (including angular momentum sources) by Eliassen (1952), who also discussed the Green's function and, hence, the transverse circulation in the vicinity of a jump in Q and a point source in Q. Eq. (2.6) is also solved numerically at each time step in balanced tropical cyclone models (e.g., Ooyama, 1969a,b; Sundqvist, 1970a,b). Some solutions of (2.6) for A, B and C determined from hurricane data have recently been presented by Willoughby (1979).

Here we are concerned with the effect of inertial stability on the spatial distribution of the local temperature change (and hence tangential wind change) produced by a specified heat source. To isolate the effects of inertial stability we consider a vortex which has constant static stability (A = constant $\equiv N^2$) and which is barotropic ($B = 0$). The radial distribution of tangential wind is assumed to be given by

$$\frac{2m}{r^2} = f + \frac{2v}{r} = \begin{cases} \hat{f} & r \leq a \\ f\left[1 + \left(\dfrac{\hat{f}^2 - f^2}{f^2}\right)\dfrac{a^4}{r^4}\right]^{1/2} & r > a, \end{cases} \tag{2.7}$$

where the vortex strength $\hat{f}$ and the radius of maximum wind a are specified constants. The corresponding absolute vorticity is

$$\frac{\partial m}{r\partial r} = f + \frac{\partial rv}{r\partial r} = \begin{cases} \hat{f} & r < a \\ f\left[1 + \left(\dfrac{\hat{f}^2 - f^2}{f^2}\right)\dfrac{a^4}{r^4}\right]^{-1/2} & r > a, \end{cases} \tag{2.8}$$

which conveniently results in the piecewise constant inertial stability parameter

$$C = \frac{\partial m^2}{r^3\partial r} = \left(f^2 + \frac{\partial rv}{r\partial r}\right)\left(f + \frac{2v}{r}\right) = \begin{cases} \hat{f}^2 & r < a \\ f^2 & r > a. \end{cases} \tag{2.9}$$

The vortex (2.7) is characterized by solid rotation inside $r = a$, while outside this radius the tangential wind decreases with radius more rapidly than the r^{-1} decrease of a Rankine vortex. In this sense it is unlike the tropical cyclone outer region, where the tangential wind decreases with radius more slowly than r^{-1}. However, our idealized barotropic vortex resembles a tropical cyclone in the sense that it has high inertial stability in the inner region and low inertial stability in the outer region. As for the heating Q, we make the simple assumption that

$$Q(r, z) = \begin{cases} 0 & 0 \leq r < b_1 \\ \hat{Q}\sin\dfrac{\pi z}{z_T} & b_1 < r < b_2 \\ 0 & b_2 < r < \infty, \end{cases} \tag{2.10}$$

where $\hat{Q}$ is a constant which gives the magnitude of the heating between b_1 and b_2. Then, assuming $\psi(r, z) = \Psi(r)\sin\dfrac{\pi z}{z_T}$, (2.6) becomes

$$\left.\begin{aligned} r^2\frac{d^2\Psi}{dr^2} + r\frac{d\Psi}{dr} - (\hat{\mu}^2r^2 + 1)\Psi = 0 \quad \text{for} \quad r < a \\ r^2\frac{d^2\Psi}{dr^2} + r\frac{d\Psi}{dr} - (\mu^2r^2 + 1)\Psi = 0 \quad \text{for} \quad r > a \end{aligned}\right\}, \tag{2.11}$$

where $\hat{\mu} = \hat{f}\pi/Nz_T$ and $\mu = f\pi/Nz_T$.

The modified Bessel equations (2.11) give rise to linear combinations of the solutions I_1 and K_1 in the four regions defined by the interior break points a, b_1 and b_2. These break points may be ordered in the following three ways:

Case 1: $b_1 < b_2 < a$,

Case 2: $b_1 < a < b_2$,

Case 3: $a < b_1 < b_2$.

Since there are linear combinations of I_1 and K_1 in four regions, eight constants must be determined for each case. The boundary conditions at the origin and infinity require that we discard K_1 for the innermost region and I_1 for the outermost region. The remaining six constants are determined by requiring

$$[\Psi]_{a-}^{a+} = [\Psi]_{b_1-}^{b_1+} = [\Psi]_{b_2-}^{b_2+} = \left[\frac{dr\Psi}{rdr}\right]_{a-}^{a+} = 0,$$

$$\left[\frac{dr\Psi}{rdr}\right]_{b_1-}^{b_1+} = (g\hat{Q}/\theta_0 N^2) \quad \text{and} \quad \left[\frac{dr\Psi}{rdr}\right]_{b_2-}^{b_2+} = -\frac{g\hat{Q}}{\theta_0 N^2}.$$

The details of this procedure for Case 2 are given in the Appendix. When the same procedure is applied to Cases 1 and 3 we then obtain the following solutions.

Case 1:

$$\Psi(r) = \frac{g\hat{Q}}{\theta_0 N^2} \begin{cases} F_1(b_1, b_1)\dfrac{I_1(\hat{\mu}r)}{I_1(\hat{\mu}b_1)} & 0 \leqslant r < b_1 \\ F_1(r, r) & b_1 < r < b_2 \\ F_1(b_2, r) & b_2 < r < a \\ F_1(b_2, a)\dfrac{K_1(\mu r)}{K_1(\mu a)} & a < r < \infty, \end{cases} \tag{2.12a}$$

where

$$F_1(x, y) = [b_2 I_1(\hat{\mu}b_2) - b_1 I_1(\hat{\mu}b_1)][\alpha I_1(\hat{\mu}y) + K_1(\hat{\mu}y)] + b_2[I_1(\hat{\mu}x)K_1(\hat{\mu}b_2) - I_1(\hat{\mu}b_2)K_1(\hat{\mu}x)];$$

Case 2:

$$\Psi(r) = \frac{g\hat{Q}}{\theta_0 N^2} \begin{cases} F_2(b_1, a)\dfrac{I_1(\hat{\mu}r)}{I_1(\hat{\mu}b_1)} & 0 \leqslant r < b_1 \\ F_2(r, a) & b_1 < r < a \\ F_2(a, r) & a < r < b_2 \\ F_2(a, b_2)\dfrac{K_1(\mu r)}{K_1(\mu b_2)} & b_2 < r < \infty, \end{cases} \tag{2.12b}$$

where

$$F_2(x, y) = b_2 K_1(\mu b_2)[I_1(\mu y) + \beta K_1(\mu y)]\frac{I_1(\hat{\mu}x)}{I_1(\hat{\mu}a)} - b_1 I_1(\mu b_1)[\alpha I_1(\hat{\mu}x) + K_1(\hat{\mu}x)]\frac{K_1(\mu y)}{K_1(\mu a)};$$

Case 3:

$$\Psi(r) = \frac{g\hat{Q}}{\theta_0 N^2} \begin{cases} F_3(b_1, a)\dfrac{I_1(\hat{\mu}r)}{I_1(\hat{\mu}a)} & 0 \leqslant r < a \\ F_3(b_1, r) & a < r < b_1 \\ F_3(r, r) & b_1 < r < b_2 \\ F_3(b_2, b_2)\dfrac{K_1(\mu r)}{K_1(\mu b_2)} & b_2 < r < \infty, \end{cases} \tag{2.12c}$$

where

$$F_3(x, y) = [b_2 K_1(\mu b_2) - b_1 K_1(\mu b_1)][I_1(\mu y) + \beta K_1(\mu y)] + b_1[I_1(\mu x)K_1(\mu b_1) - I_1(\mu b_1)K_1(\mu x)].$$

Here we have defined

$$\alpha = \frac{\hat{\mu}K_0(\hat{\mu}a)K_1(\mu a) - \mu K_0(\mu a)K_1(\hat{\mu}a)}{\hat{\mu}I_0(\hat{\mu}a)K_1(\mu a) + \mu I_1(\hat{\mu}a)K_0(\mu a)},$$

$$\beta = \frac{\mu I_0(\mu a)I_1(\hat{\mu}a) - \hat{\mu}I_0(\hat{\mu}a)I_1(\mu a)}{\mu K_0(\mu a)I_1(\hat{\mu}a) + \hat{\mu}I_0(\hat{\mu}a)K_1(\mu a)}.$$

Let us now determine the radial distribution of local temperature change. Since our assumed vortex is barotropic (i.e., $\partial\theta/\partial r = 0$) the thermodynamic equation simplifies to

$$\frac{\partial\theta}{\partial t} = Q - \frac{\theta_0}{g} N^2 w, \tag{2.13}$$

which shows that the local warming equals the difference between the specified heating and the adiabatic cooling associated with the forced secondary circulation. If we use (2.12) to determine w, and if we evaluate (2.13) at $z = z_T/2$, we obtain the following.

Case 1:

$$\frac{\partial\theta}{\partial t}\left(r, \frac{z_T}{2}\right) = \hat{Q} \begin{cases} G_1(b_1, b_1)\dfrac{I_0(\hat{\mu}r)}{I_0(\hat{\mu}b_1)} & 0 \leqslant r < b_1 \\ G_1(r, r) & b_1 < r < b_2 \\ G_1(b_2, r) & b_2 < r < a \\ G_1(b_2, a)\dfrac{K_0(\mu r)}{K_0(\mu a)} & a < r < \infty, \end{cases} \tag{2.14a}$$

[3] The reader wishing to check the results (2.12a–c) can do so without going through the complete derivation. One can easily verify that (2.12a–c) are solutions of (2.11) and that $\Psi(r)$ is continuous at $r = a$, b_1 and b_2. The matching conditions on $dr\Psi/rdr$ can then be verified by using the two derivative relations and the Wronskian given in the Appendix.

where

$$G_1(x, y) = 1 + [\hat{\mu}b_1 I_1(\hat{\mu}b_1) - \hat{\mu}b_2 I_1(\hat{\mu}b_2)][\alpha I_0(\hat{\mu}y) - K_0(\hat{\mu}y)] - \hat{\mu}b_2[I_0(\hat{\mu}x)K_1(\hat{\mu}b_2) + I_1(\hat{\mu}b_2)K_0(\hat{\mu}x)];$$

Case 2:

$$\frac{\partial\theta}{\partial t}\left(r, \frac{z_T}{2}\right) = \hat{Q}\begin{cases} G_2(b_1, a)\dfrac{I_0(\hat{\mu}r)}{I_0(\hat{\mu}b_1)} & 0 \leqslant r < b_1 \\ G_2(r, a) & b_1 < r < a \\ G_2(a, r) & a < r < b_2 \\ G_2(a, b_2)\dfrac{K_0(\mu r)}{K_0(\mu b_2)} & b_2 < r < \infty, \end{cases} \tag{2.14b}$$

where

$$G_2(x, y) = 1 + \hat{\mu}b_1 I_1(\hat{\mu}b_1)[\alpha I_0(\hat{\mu}x) - K_0(\hat{\mu}x)] \times \frac{K_0(\mu y)}{K_0(\mu a)} - \mu b_2 K_1(\mu b_2)[I_0(\mu y) - \beta K_0(\mu y)]\frac{I_0(\hat{\mu}x)}{I_0(\hat{\mu}a)};$$

Case 3:

$$\frac{\partial\theta}{\partial t}\left(r, \frac{z_T}{2}\right) = \hat{Q}\begin{cases} G_3(b_1, a)\dfrac{I_0(\hat{\mu}r)}{I_0(\hat{\mu}a)} & 0 \leqslant r < a \\ G_3(b_1, r) & a < r < b_1 \\ G_3(r, r) & b_1 < r < b_2 \\ G_3(b_2, b_2)\dfrac{K_0(\mu r)}{K_0(\mu b_2)} & b_2 < r < \infty, \end{cases} \tag{2.14c}$$

where

$$G_3(x, y) = 1 + [\mu b_1 K_1(\mu b_1) - \mu b_2 K_1(\mu b_2)][I_0(\mu y) - \beta K_0(\mu y)] - \mu b_1[I_0(\mu x)K_1(\mu b_1) + I_1(\mu b_1)K_0(\mu x)].$$

According to (2.12) and (2.14) the radial distributions of $(\theta_0 N^2/g)\psi$ and $\partial\theta/\partial t$ depend on the six parameters a, b_1, b_2, $\hat{\mu}$, μ, $\hat{Q}$. We shall henceforth assume $\mu^{-1} = 1000$ km. As for the choice of $\hat{Q}$ we shall relate it to b_1 and b_2 by assuming that the total heating over the whole domain, $\int_0^{z_T}\int_0^{\infty} Q r dr dz$, is a constant.[4] This assumption can be written

$$\hat{Q}(b_2^2 - b_1^2) = \text{constant} \equiv (10°\text{C day}^{-1})\cdot(250\text{ km})^2, \tag{2.15}$$

[4] From (2.13) and the boundary conditions on ψ we can show that the total warming over the whole domain, $\int_0^{z_T}\int_0^{\infty}\frac{\partial\theta}{\partial t} r dr dz$, is equal to the same constant. To avoid confusion please note that we are using the term "heating" in reference to Q and the term "warming" in reference to $\partial\theta/\partial t$.

TABLE 1. The radial distribution of rainfall (cm day^{-1}) by two-degree radial bands for both Atlantic and Pacific composite storms. Note that intensification is accompanied by increased rainfall in the inner region but little change in the area averaged rainfall. Data taken from Gray (1981).

	0–2°	2–4°	4–6°	6–8°	8–10°	Area average
Pre-hurricane	1.9	1.5	0.9	0.5	0.5	0.76
Hurricane	6.3	2.0	0.7	0.3	0.4	0.86
Pre-typhoon	3.4	2.6	1.5	0.7	0.7	1.20
Typhoon	8.3	2.3	0.1	0.8	0.7	1.10

where we have chosen the constant so that a circular region 250 km in radius has a heating rate of 10°C day^{-1}. One interpretation of (2.15) is that it is simply a way of normalizing our results so that the radial distribution of local warming $\partial\theta/\partial t$ will vary with a, b_1, b_2 and $\hat{\mu}$ but the total warming over the domain will remain fixed. Another interpretation is that as the annular area of precipitation decreases in size, the local rainfall rate increases in such a way that the total amount of processed water remains constant. As evidence that this is roughly in accord with observations, we present in Table 1 the radial distribution of rainfall (cm day^{-1}) as given by Gray (1981) for pre-hurricanes and pre-typhoons (maximum winds $\leqslant$ 10–15 m s^{-1}) versus hurricanes and typhoons (maximum winds $>$ 33 m s^{-1} or minimum central pressure $<$ 980 mb). The rainfall rates were determined from heat budget analysis on upper air data which had been composited by two-degree radial bands. Of interest here is how intensification is accompanied by increased rainfall in the inner region and decreased rainfall in the outer region so that the area averaged rainfall shows little variation.

With the above assumptions on μ and $\hat{Q}$ we proceed in the next section to study the dependence of ψ and $\partial\theta/\partial t$ on the inertial stability parameters $\hat{\mu}$, a and the heating parameters b_1, b_2.

3. Effects of inertial stability and heating distribution

In order to determine reasonable values for the parameters a, b_1, b_2 and $\hat{\mu}$ let us consider the "typical" time development of central surface pressure and maximum tangential wind shown in Fig. 2. Those curves have been constructed so as to be consistent with the observational results of Shea and Gray (1973) and Holliday and Thompson (1979). Shea and Gray analysed 533 radial leg aircraft flights made by the National Hurricane Research Project and established an empirical relation between central surface pressure and maximum tangential wind. Holliday and Thompson studied 305 typhoons occurring over a 21 year period and found that 50% had deepening rates greater than 24 mb day^{-1}, 25% had rates greater than 43 mb day^{-1} and 23% had

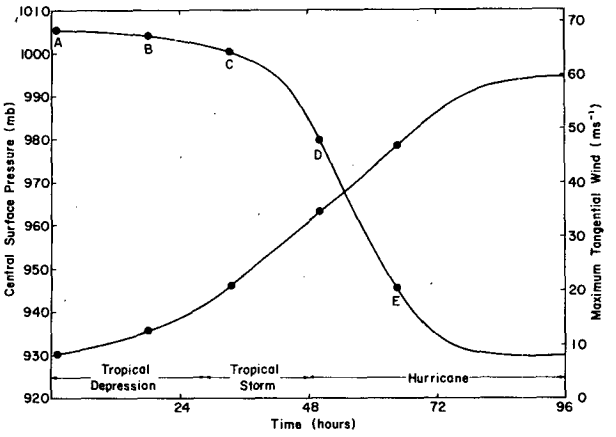

FIG. 2. "Typical" tropical cyclone time development of central surface pressure and maximum tangential wind. The points labeled A–E correspond roughly to the specified parameters and results shown in Table 2.

eventual surface pressures lower than 920 mb. One might regard Fig. 2 as being typical of the more intense 25–30% of typhoons.

Now consider the points A through E along the curves in Fig. 2. Observations show that as a cyclone develops, the size of the region of high inertial stability decreases while the magnitude of the inertial stability increases. In addition, the outer boundary of the convectively active region contracts and an eye forms. Because our inertial stability and heating distributions are so idealized, the choice of numerical values for a, b_1, b_2 and $\hat{\mu}$ is not straightforward. A set of values which we believe is roughly in accord with observations is given in columns 2–5 of Table 2. With these values of the inertial stability and heating parameters we shall now discuss four phenomena which our solutions help illustrate: stiffening, collapse of the radius of maximum wind, changing efficiency during cyclone development, and the stabilizing effect of eye formation.

a. *Stiffening*[5]

We first demonstrate that an increase in inertial stability leads to a decrease in the forced secondary circulation and a change in the radial distribution of the warming. Consider the case $b_1 = 0$ and $b_2 = 250$ km. Isolines of $r\psi$ and $\partial\theta/\partial t$ computed from (2.12)[6] and (2.14) for the case $\hat{\mu} = \mu$ (zero relative vorticity) are shown in Figs. 3a and 3b.[7] The heating forces upward motion inside 250 km, with weak subsidence in the broad outlying region. Inside 250 km the cooling due to adiabatic ascent nearly balances the heating so that only slight warming results. Outside 250 km subsidence produces slight warming. Thus, Fig. 3b shows that cluster-scale convective heating of the tropical atmosphere in a region with very weak relative vorticity results in small temperature changes over a broad area. Figs. 3c and 3d have also been constructed from (2.12) and (2.14) using $b_1 = 0$ and $b_2 = 250$ km but with $(\hat{\mu} - \mu)/\mu = 5$ and $a = 200$ km. These values are close to those for stage C in Table 2. In comparing Figs. 3a and 3c we note that there is only a slight suppression of the forced secondary circulation when $\hat{\mu}$ changes from μ to 6μ. In fact the average vertical mass flux inside 200 km is reduced by only 14%. However, this is enough to result in a fivefold increase in $\partial\theta/\partial t$ inside 100 km. Thus, although the area averaged warming is the same in Figs. 3b and 3d, the radial distribution of $\partial\theta/\partial t$ is quite different.

TABLE 2. Typical values of the parameters a, b_1, b_2 and $\hat{\mu}$ for the stages A–E shown in Fig. 2.

Stage	a (km)	b_1 (km)	b_2 (km)	$\frac{\hat{\mu}-\mu}{\mu}$
A	300	0	250–350	0
B	250	0	200–300	2
C	200	0	150–250	4
D	150	0–30	100–200	10
E	100	0–30	50–150	24

From this example there emerges the following physical picture. When the relative vorticity is small compared to f there is little resistance to the movement of air in the (r, z) plane and there is so much vertical motion that the N^2w term in the thermodynamic equation nearly cancels the Q term. As the relative vorticity begins to exceed f the vortex stiffens and the forced secondary circulation is reduced. The warming in the high inertial stability inner region becomes larger while that in the low inertial stability outer region becomes smaller. Thus, somewhat surprisingly, it appears that the transverse circulation can weaken at the same time the tangential wind and horizontal temperature gradient are increasing more and more rapidly.[8]

b. *Collapse of the radius of maximum wind*

An interesting feature implied by Fig. 3d is a small lower tropospheric tangential wind change for the $200 < r < 250$ km part of the heated region and a

[5] An excellent qualitative discussion of this effect has been given by Ooyama (1982). The role of potential vorticity as a measure of stiffness in the formation of fronts and jets has been discussed by Hoskins (1974).

[6] For the evaluation of (2.12) we have chosen $g = 9.8$ m s^{-1}, $\theta_0 = 298$ K, and $N = 1.2 \times 10^{-2}$ s^{-1}.

[7] Note that the value of a is irrelevant when $\hat{\mu} = \mu$.

[8] Professor Kerry Emanuel has pointed out that, while increased inertial stability suppresses the transverse circulation associated with the heating, it also implies larger transverse circulation associated with boundary layer pumping. We are presently using an axisymmetric primitive equation model to study this effect.

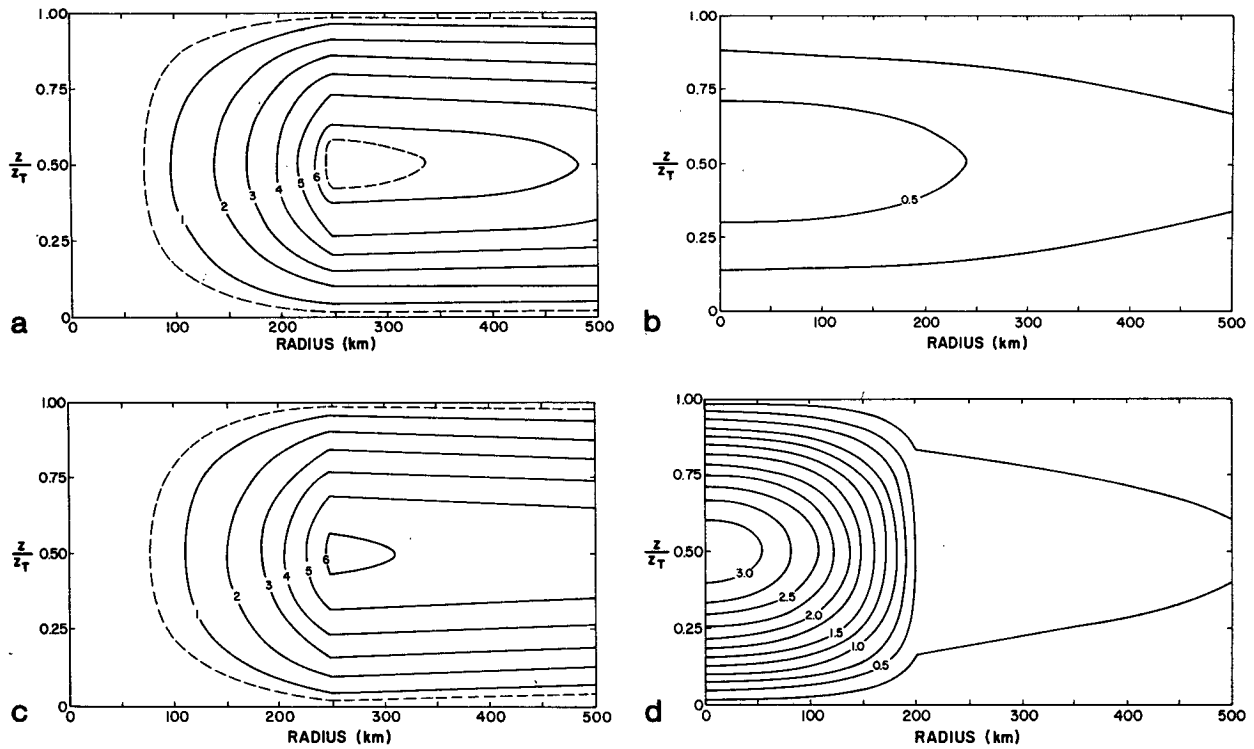

FIG. 3. Transverse circulation and warming when a = 200 km, b_1 = 0, b_2 = 250 km, and $\hat{\mu}$ is either μ or 6μ. (a) $r\psi(r, z)$ for $\hat{\mu} = \mu$; (b) $\partial\theta/\partial t$ for $\hat{\mu} = u$; (c) $r\psi(r, z)$ for $\hat{\mu} = 6\mu$; (d) $\partial\theta/\partial t$ for $\hat{\mu} = 6\mu$. The units on $r\psi(r, z)$ are 10^{13} m^3 day^{-1} while those on $\partial\theta/\partial t$ are °C day^{-1}. Note that there is only a slight suppression of the transverse circulation but a large enhancement of $\partial\theta/\partial t$ when $\hat{\mu}$ changes from μ to 6μ.

large change inside 200 km. Apparently, larger cyclonic lower tropospheric tangential accelerations will appear where the inertial stability is larger. This response can be deduced if one recalls that the vortex will at all times satisfy thermal wind balance, which would require an immediate response of the momentum field to any changes produced in the temperature field.

Imagine a tropical disturbance which is weak but fairly symmetric and which has heating both inside and outside the radius of maximum wind. Since the inertial stability is larger just inside the radius of maximum wind, the lower tropospheric tangential acceleration will be larger there. Also note that the gradient of the inertial stability is usually quite large in the vicinity of the radius of maximum wind, such that a corresponding gradient of tangential acceleration should be expected. The result of such a distribution of heating and inertial stability would be an apparent inward movement of the radius of maximum wind. That is, fluid particles just inside the radius of maximum wind will experience a larger acceleration than fluid particles just at or beyond this radius, giving the appearance of an inward shift or collapse of the peak winds. From the above argument, one can picture the tendency for the radius of maximum wind to move inward until it coincides with the inner edge of the heated region. This ten-

TABLE 3. Table of parameters used to construct Fig. 4 (b_1 = 0), and assumed values of $\hat{Q}$ to allow a dimensional interpretation. Note that the area-averaged Q is the same for all five stages shown in the table. The effective precipitation rates are what would occur for the corresponding assumed $\hat{Q}$.

Stage	a or b_2 (km)	$\frac{\hat{\mu}-\mu}{\mu}$	$\hat{Q}$ (°C day^{-1})	Effective precipitation rate (mm day^{-1})	$\frac{\partial\theta/\partial t}{\hat{Q}}$ at $r = 0$	$\frac{\partial\theta}{\partial t}$ at $r = 0$ (°C day^{-1})
A	300	0	6.94	16.3	0.083	0.58
B	250	2	10.00	23.5	0.167	1.67
C	200	4	15.63	36.7	0.236	3.69
D	150	10	27.78	65.2	0.456	12.67
E	100	24	62.50	146.7	0.698	43.63

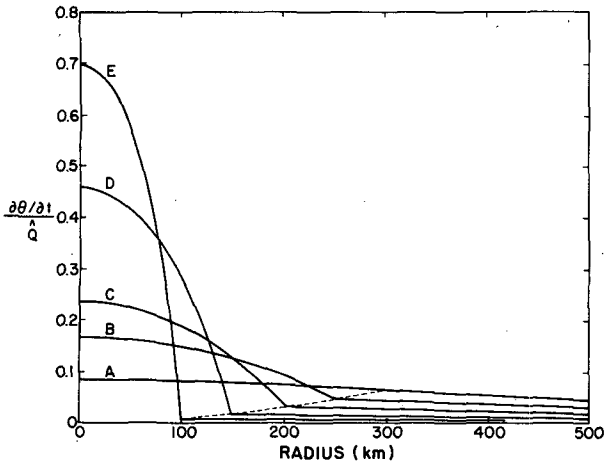

FIG. 4. The radial distribution of $\partial\theta/\partial t/\hat{Q}$ for the five stages of tropical cyclone development given in Table 3.

dency for contraction of the radius of maximum wind is also discussed by Shapiro and Willoughby (1981) and Willoughby *et al.* (1982).

c. *Changing efficiency during tropical cyclone development*

Next we examine the effect of changing inertial stability on tropical cyclone development. We begin by presenting, in Fig. 4, some examples of the radial distribution of normalized local temperature change for the five stages of tropical cyclone development shown in Fig. 2. These results have been obtained by evaluating (2.14) with $b_1 = 0$, $b_2 = a$ and the values of a and $\hat{\mu}$ specified in Table 3. This diagram shows the remarkable increase in efficiency which accompanies increased inertial stability. This large increase in efficiency contributes to an even larger increase in local warming rates, as can be seen in Table 3. In the sixth column we have listed the $r = 0$ values of $(\partial\theta/\partial t)/\hat{Q}$ which appear in Fig. 4. Assuming that the total heating over the whole domain is a constant [see (2.15)] we obtain the values of $\hat{Q}$ shown in the fourth column. Multiplying these two quantities we obtain the dimensional local warming rates at $r = 0$ which are given in the last column.[9] The combination of increased efficiency and increased $\hat{Q}$ is seen to result in a 75-fold increase in the warming rate.

The increase in heating efficiency for stages A through E is entirely a consequence of the increased inertial stability of the vortex. A more concise way of demonstrating this effect is to calculate the average fraction of heating which ends up as local temperature change in the region $0 \leqslant r \leqslant b_2$. Integrating (2.13) over the heated region, using the relations $\int_0^{b_2} w\, r dr = b_2\Psi(b_2)\sin(\pi z/z_T)$, (2.10), (2.12) and normalizing by the heating, we obtain

$$\frac{\int_0^{b_2}\frac{\partial\theta}{\partial t}rdr}{\int_0^{b_2}Qrdr} = \begin{cases} 1 - 2I_1(\hat{\mu}b_2)[\alpha I_1(\hat{\mu}b_2) + K_1(\hat{\mu}b_2)] \\ \qquad a > b_2 \\ 1 - 2K_1(\mu b_2)[I_1(\mu b_2) + \beta K_1(\mu b_2)] \\ \qquad a < b_2\,. \end{cases} \tag{3.1}$$

Fig. 5 shows isolines of this integrated heating efficiency as a function of the inertial stability $(\hat{\mu} - \mu)/\mu$ and the size of the inertially stable region a. The outer boundary of the heated region, b_2, is assumed to be 50 km greater than a in Fig. 5a and 50 km smaller in Fig. 5b. The stippled area on both diagrams represents one possible path a tropical cyclone might take in its development, with stages A through E labeled for reference. When these diagrams are compared it is clear that the more efficient configuration is the one in which the heated region is confined within the inertially stable region. Qualitatively though, the diagrams are very similar. Note the rapid increase in efficiency which occurs between stages C and D in both diagrams. During this period the inertially stable region collapses in size, but the inertial stability parameter increases. We see from these figures that the collapse of the inertially stable region (and heated region) always results in a decrease in efficiency. Thus, it is the increase in the inertial stability of the vortex which accounts for the increase in efficiency shown in Figs. 4 and 5. It is worth mentioning that the rapid increase in efficiency between stages C and D corresponds to the point at which a tropical cyclone would begin a period of rapid intensification. One might infer from this diagram that this period of rapid intensification results from a more efficient use of the convective heating, rather than from an increase in convection. This type of nonlinear interaction of the heating and motion field is not addressed by the original linear CISK hypothesis, and it makes linear theory inapplicable to stages of tropical cyclone development beyond the tropical depression phase.

d. *Effect of eye formation*

To illustrate the effect of eye formation we have plotted in Fig. 6 the radial distribution of

$$\frac{\partial\theta/\partial t}{\left(1 - \frac{b_1^2}{b_2^2}\right)\hat{Q}} \quad \text{for} \quad \frac{\hat{\mu} - \mu}{\mu} = 24,$$

$a = b_2 = 100$ km and $b_1 = 0$, 10, 20, 30 km. These parameters correspond to stage E of Table 3 and Fig. 2. Because of (2.15) the normalizing factor $[1 - (b_1^2/b_2^2)]\hat{Q}$ does not vary as b_1 varies. Fig. 6 shows

[9] The increased warming rates should be interpreted only as an effect of increased inertial stability. Other processes that might tend to stabilize the vortex are not included in our analysis.

that, even though the heating $\hat{Q}$ increases as b_1 increases, the local temperature change decreases. In this sense one can regard the formation of an eye as a process which tends to stabilize the vortex. One interpretation of this effect is that the formation of an eye removes heating in the region most remote from the outlying low inertial stability region and adds heating in the region adjacent to the low inertial stability region. In actual tropical cyclones the inertial stability increases as one approaches the center, a situation which would apparently produce an even stronger effect.

4. Concluding remarks

The linear CISK theories of Ooyama (1964, 1969a) and Charney and Eliassen (1964) have provided an important conceptual understanding of certain aspects of tropical cyclone development. The growth of the cyclone-scale circulation in these theories is linearly coupled to an increase in cumulus convection, precipitation, and hence convective heating, while the inertial stability remains essentially f^2. Observations (e.g., Gray, 1981) and numerical simulations using nonlinear models do not appear to support this physical picture. This raises the question of what other processes might be contributing to the rapid growth of the tropical cyclone. Using a simple diagnostic analysis we have demonstrated the important role inertial stability plays in enabling latent heat release to produce local temperature change and hence tangential wind change. This study suggests that local warming by cumulus convection is considerably greater if the convection is confined to a region of relatively high inertial stability. The collapse of the vortex also appears to be linked to the heating by convection inside the high inertial stability region. During the period of rapid intensification, the nonlinear feedback between this increasing efficiency and increasing inertial stability apparently plays a major role in hurricane development. The formation of an eye during the later stages of development appears to have a stabilizing effect on the vortex.

Presently, the ability to forecast which tropical depressions will develop into hurricanes or typhoons is rather poor. The theoretical results presented here suggest that observational studies should concentrate on the relation of the inertial stability distribution and the cloud population.

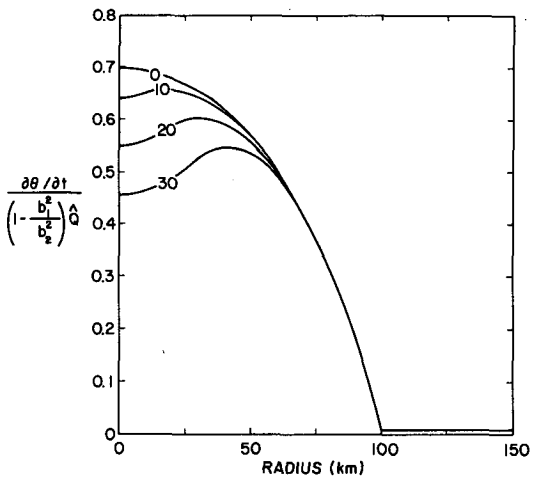

FIG. 6. The radial distribution of $(\partial\theta/\partial t)/[1 - (b_1^2/b_2^2)]\hat{Q}$ for $(\hat{\mu} - \mu)/\mu = 24$, $a = b_2 = 100$ km and $b_1 = 0$, 10, 20, 30 km.

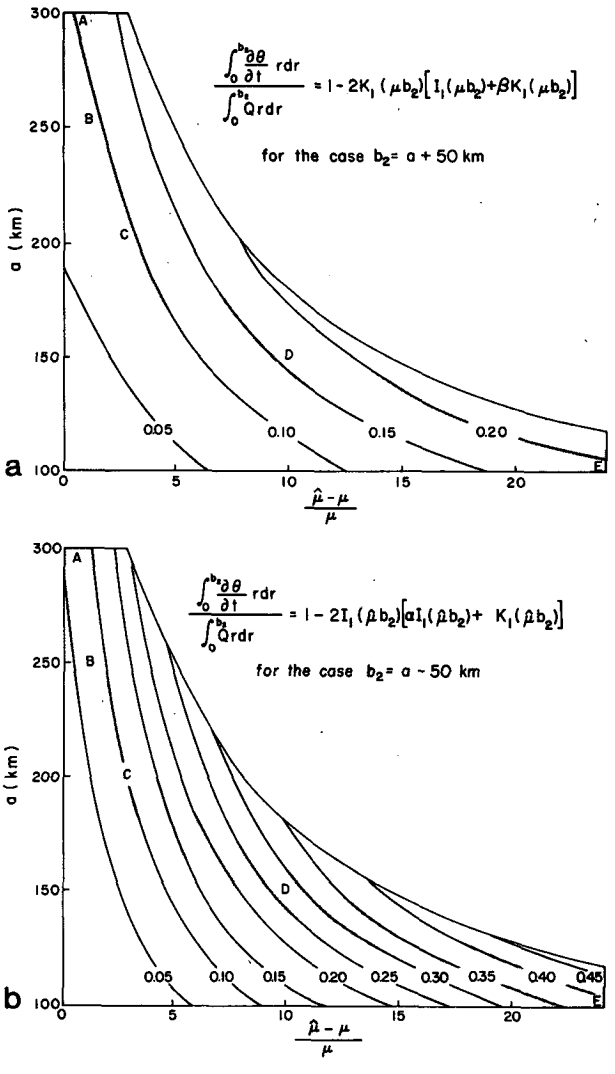

FIG. 5. Isolines of $\int_0^{b_2} \frac{\partial\theta}{\partial t} rdr \Big/ \int_0^{b_2} Q\, rdr$ in the $(a, \hat{\mu} - \mu/\mu)$ plane for (a) $b_2 = a + 50$ km and (b) $b_2 = a - 50$ km. The stippled area represents the path a developing tropical storm might follow, with stages A–E (see Table 2 and Fig. 2) labeled for reference.

Acknowledgments. The authors are grateful to Scott Fulton, Mark DeMaria, William Gray, Duane Stevens, Kerry Emanuel, Lloyd Shapiro and Vic Ooyama for their valuable comments on this problem. We are also indebted to Odilia Panella for her help in preparing the manuscript. This research was supported by NSF Grant ATM-8009799 and ONR Grant N00014-79-C-0793.

APPENDIX

Derivation of the Solution of (2.11), Case 2

We outline here the derivation of the solution of (2.11) for Case 2 ($b_1 < a < b_2$). The solution can be written

$$\Psi(r) = \frac{g\hat{Q}}{\theta_0 N^2} \begin{cases} [AI_1(\hat{\mu}b_1) + BK_1(\hat{\mu}b_1)] \dfrac{I_1(\hat{\mu}r)}{I_1(\hat{\mu}b_1)} & 0 \leqslant r < b_1 \\ AI_1(\hat{\mu}r) + BK_1(\hat{\mu}r) & b_1 < r < a \\ CI_1(\mu r) + DK_1(\mu r) & a < r < b_2 \\ [CI_1(\mu b_2) + DK_1(\mu b_2)] \dfrac{K_1(\mu r)}{K_1(\mu b_2)} & b_2 < r < \infty, \end{cases} \tag{A1}$$

where we have used the boundary conditions at the origin and infinity to discard $K_1(\hat{\mu}r)$ in the inner region and $I_1(\mu r)$ in the outer region. In addition we have written (A1) in such a way that Ψ is already continuous at b_1 and b_2. The four constants A, B, C, D can now be determined from the matching conditions for Ψ at $r = a$ and $dr\Psi/rdr$ at $r = b_1, a, b_2$. Using the derivative relations $(d/rdr)[rI_1(\lambda r)] = \lambda I_0(\lambda r)$ and $(d/rdr)[rK_1(\lambda r)] = -\lambda K_0(\lambda r)$, we can differentiate (A1) to obtain

$$\frac{dr\Psi}{rdr} = \frac{g\hat{Q}}{\theta_0 N^2} \begin{cases} \hat{\mu}[AI_1(\hat{\mu}b_1) + BK_1(\hat{\mu}b_1)] \dfrac{I_0(\hat{\mu}r)}{I_1(\hat{\mu}b_1)} & 0 \leqslant r < b_1 \\ \hat{\mu}[AI_0(\hat{\mu}r) - BK_0(\hat{\mu}r)] & b_1 < r < a \\ \mu[CI_0(\mu r) - DK_0(\mu r)] & a < r < b_2 \\ -\mu[CI_1(\mu b_2) + DK_1(\mu b_2)] \dfrac{K_0(\mu r)}{K_1(\mu b_2)} & b_2 < r < \infty. \end{cases} \tag{A2}$$

With the help of the Wronskian $I_0(z)K_1(z) + K_0(z)I_1(z) = 1/z$ we can derive from the jump condition $[dr\Psi/rdr]_{b_1^-}^{b_1^+} = g\hat{Q}/\theta_0 N^2$ the result

$$B = -b_1 I_1(\hat{\mu}b_1). \tag{A3}$$

Similarly, from the jump condition $[dr\Psi/rdr]_{b_2^-}^{b_2^+} = -g\hat{Q}/\theta_0 N^2$ we obtain

$$C = b_2 K_1(\mu b_2). \tag{A4}$$

The constants A and D are now determined by requiring that Ψ and $dr\Psi/rdr$ be continuous at $r = a$. The results are

$$A = b_2 K_1(\mu b_2)[I_1(\mu a) + \beta K_1(\mu a)] \frac{1}{I_1(\hat{\mu}a)} - b_1 I_1(\hat{\mu}b_1)\alpha, \tag{A5}$$

$$D = b_2 K_1(\mu b_2)\beta - b_1 I_1(\hat{\mu}b_1)[\alpha I_1(\hat{\mu}a) + K_1(\hat{\mu}a)] \frac{1}{K_1(\mu a)}. \tag{A6}$$

Using the results (A3)–(A6) we can write our final solution as

$$\Psi(r) = \frac{g\hat{Q}}{\theta_0 N^2} \begin{cases} \left\{ b_2 K_1(\mu b_2)[I_1(\mu a) + \beta K_1(\mu a)] \dfrac{I_1(\hat{\mu}b_1)}{I_1(\hat{\mu}a)} - b_1 I_1(\hat{\mu}b_1)[\alpha I_1(\hat{\mu}b_1) + K_1(\hat{\mu}b_1)] \right\} \dfrac{I_1(\hat{\mu}r)}{I_1(\hat{\mu}b_1)}, & 0 \leqslant r < b_1 \\ \left\{ b_2 K_1(\mu b_2)[I_1(\mu a) + \beta K_1(\mu a)] \dfrac{I_1(\hat{\mu}r)}{I_1(\hat{\mu}a)} - b_1 I_1(\hat{\mu}b_1)[\alpha I_1(\hat{\mu}r) + K_1(\hat{\mu}r)] \right\}, & b_1 < r < a \\ \left\{ b_2 K_1(\mu b_2)[I_1(\mu r) + \beta K_1(\mu r)] - b_1 I_1(\hat{\mu}b_1)[\alpha I_1(\hat{\mu}a) + K_1(\hat{\mu}a)] \dfrac{K_1(\mu r)}{K_1(\mu a)} \right\}, & a < r < b_2 \\ \left\{ b_2 K_1(\mu b_2)[I_1(\mu b_2) + \beta K_1(\mu b_2)] - b_1 I_1(\hat{\mu}b_1) \times [\alpha I_1(\hat{\mu}a) + K_1(\hat{\mu}a)] \dfrac{K_1(\mu b_2)}{K_1(\mu a)} \right\} \dfrac{K_1(\mu r)}{K_1(\mu b_2)}, & b_2 < r < \infty. \end{cases} \tag{A7}$$

Using the definition of F_2 this solution easily converts to the form given in (2.12b).

REFERENCES

Charney, J. G., and A. Eliassen, 1964: On the growth of the hurricane depression. *J. Atmos. Sci.*, **21,** 68–75.

Eliassen, A., 1952: Slow thermally or frictionally controlled meridional circulation in a circular vortex. *Astrophys. Norv.*, **5,** 60 pp.

Gray, W. M., 1981: *Recent advances in tropical cyclone research from rawinsonde composite analysis.* WMO, 407 pp.

Holliday, C. R., and A. H. Thompson, 1979: Climatological characteristics of rapidly intensifying typhoons. *Mon. Wea. Rev.*, **107,** 1022–1034.

Hoskins, B. J., 1974: The role of potential vorticity in symmetric stability and instability. *Quart. J. Roy. Meteor. Soc.*, **100,** 480–482.

——, and F. P. Bretherton, 1972: Atmospheric frontogenesis models: Mathematical formulation and solution. *J. Atmos. Sci.*, **29,** 11–37.

Ooyama, K., 1964: A dynamical model for the study of tropical cyclone development. *Geofis. Int.*, **4,** 187–198.

——, 1969a: Numerical simulation of the life cycle of tropical cyclones. *J. Atmos. Sci.*, **26,** 3–40.

——, 1969b: Numerical simulation of tropical cyclones with an axisymmetric model. *Proc. WMO/IUGG Symp. on Numerical Weather Prediction*, Tokyo, 1968, III: 81–88.

——, 1982: Conceptual evolution of the theory and modeling of the tropical cyclone. *J. Meteor. Soc. Japan,* **60,** 369–379.

Shapiro, L. J., and H. E. Willoughby, 1982: The response of balanced hurricanes to local sources of heat and momentum. *J. Atmos. Sci.*, **39,** 378–394.

Shea, D. J., and W. M. Gray, 1973: The hurricane's inner core region, I: Symmetric and asymmetric structure. *J. Atmos. Sci.*, **30,** 1544–1564.

Smith, R., 1981: The cyclostrophic adjustment of vortices with application to tropical cyclone modification. *J. Atmos. Sci.*, **38,** 2021–2030.

Sundqvist, H., 1970a: Numerical simulation of the development of tropical cyclones with a ten-level model. Part I. *Tellus*, **22,** 359–390.

——, 1970b: Numerical simulation of the development of tropical cyclones with a ten-level model. Part II. *Tellus*, **22,** 504–510.

Willoughby, H. E., 1979: Forced secondary circulations in hurricanes. *J. Geophys. Res.*, **84,** 3173–3183.

——, J. Clos and M. Shoreibah, 1982: Concentric eye walls, secondary wind maxima and the evolution of symmetric hurricane vortices. *J. Atmos. Sci.*, **39,** 395–411.